Design and Applications of a Toroidal Grating Beamline

A. Rubens B. de Castro[1] P. T. Fonseca[1] J. G. Pacheco
J. E. Verdugo, M. S. Z. Graeff[1], G. B. Fraguas[1]

Laboratório Nacional de Luz Síncrotron/CNPq, Caixa Postal 6192, 13081-970, Campinas, SP, Brasil

[1] *also at Instituto de Física "Gleb Wataghin", Universidade Estadual de Campinas Caixa Postal 6165, 13081-970, Campinas, SI;*

Received December 11, 1992

The National Synchrotron Light Laboratory (LNLS) has designed and built a beamline for vacuum ultraviolet photons in the spectral range from 12 to 310 eV, based on toroidal optical elements. The beamline was installed at the Center for Advanced Microstructures and Devices/Lousiana State University (CAMD/LSU) for testing, and saw synchrotron light for the first time on 19 October 1992. Commissioning is currently underway. Tolerance requirements for optical alignment will be discussed and correlated to the optical performance observed on initial operation of the beamline at CAMD. At the ultimate stored current expected at CAMD (400 mA@1.2 GeV) the heat load on the beamline will exceed initial design parameters by a large factor. As remedial action a water cooled chamber for the first mirror is being built at LNLS. A standard UVH compatible slit assembly will also be modified to allow for active cooling. The thermal design relied, in both cases, on ray-tracing coupled to finite-element computer programs. A secondary instrument for the spectral range 39-180 eV was built at LNLS using a small toroidal grating and a focal plane array detector system. It will be coupled to the LNLS/CAMD beamline in Dec 1992. The expected photon flux, spectral range and resolution are well suited to applications in chemistry and physics. Soft X-ray fluorescence experiments on boron and beryllium compounds are scheduled for early 993. Signal strength estimates show that these measurements can be done at the Toroidal Grating Monochromator (TGM) beamline installed at CAMD.

I. Introduction

The National Synchrotron Light Laboratory (LNLS)[1] has designed and built a beamline for vacuum ultraviolet photons in the range 12 eV thru 310 eV, based on a toroidal grating monochromator and toroidal mirrors[2]. This beamline has been shipped to the Center for Advanced Microstructures and Devices/Lousiana State University (CAMD/LSU)[3] on July 1992 and saw synchrotron light the first time on October 1992. Secondary instruments are currently being mounted to its sample chamber; commissioning of this beamline is underway and scientific applications are expected to start in the beginning of 1993.

Figure 1 shows the beamline, as configured to CAMD. On the left side of the concrete shield wall one sees safety devices belonging to the beamline front-end, and the prefocussing MIRROR 1 chamber. The source virtual centrr is indicated at the extreme left corner of the drawing.

To the right side of the concrete shield wall one sees the optical components of the beamline proper. The photon beam is collimated (by MIRROR 1) on the ENTRANCE SLITS, then shines on the TOROIDAL GRATING and is dispersed spectrally. A spectral band of width ΔE passes thru the EXIT SLITS, and is refocussed by MIRROR 2 onto a sample sitting on the center of the SAMPLE CHAMBER.

There are no windows between the synchrotron source and the sample because none of the known solid materials is transparent to the spectral range of interest. The whole bearnline is therefore at a vacuum in the 10^{-10} mbar range. The vacuum design of the beamline has been discussed elsewhere[4]. The main requirement is that the bearnline be free from hydrocarbons, hence ion pumping is used everywhere, and suitable cleaning/assembly procedures are followed.

The expected photon flux (2×10^{11} ph/sec, 0.1% band pass @ 1.15 GeV and 0.1A), spectral range (12 eV to 310 eV) and resolution ($E/\Delta E \sim 500$ to 1000) are suitable to a variety of applications in chemistry (photo-induced reactions in gas phase, photo emission in solid and gas phases) and physics (photo-emission and X-ray fluorescent in light atomic species, surface states, conduction and valence band studies, etc). A VUV spectrograph with toroidal grating and focal plane array detector was also built at LNLS and is currently being mounted to the sample chamber of this beamline. It will be used for studies in boron and beryllium compounds.

In the rest of this article we will (i) review the op-

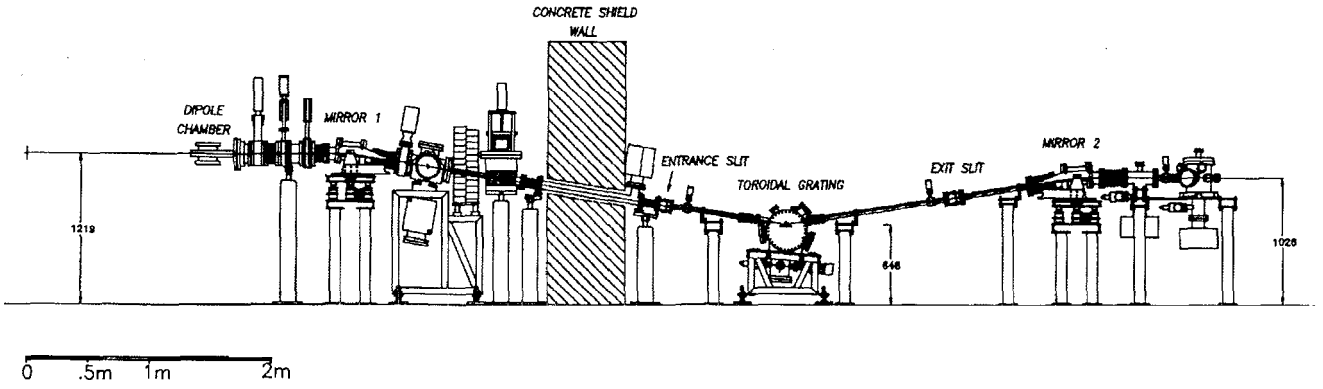

Figure 1: The LNLS TGM beamline, as installed at CAMD (Baton Rouge-USA)

tical design of the beamline, with emphasis on tolerante requirements for successful optical alignment; (ii) discuss the optical performance of this beamline under thermal loads typical of operation at CAMD at high stored current; (iii) describe the secondary instrument built at LNLS for X-ray fluorescence studies and outline the research which we intend to perform with it.

II. Optical considerations

11.1. Reflectivity

The outstretched shape of most beamlines for synchrotron radiation is imposed by the vanishing reflectivity of any mirror coating at near normal incidence, for photon energies above a few dozen eV. One is therefore forced to design optical elements (mirrors and gratings) for grazing incidence at very shallow angles in order to keep absorption losses within manageable bounds.

At high photon energies the dielectric function of all solids differs from unity by small real and imaginary parts. One finds that for a given photon energy, the reflectivity is large only for grazing angles of incidente shallower than a critical value. Figure 2 shows the reflectivity of gold for the spectral range of interest at representative angles, cornputed with SHADOW[5]. Notice the losses at large energy and large angles.

The surface finish of the mirror affects the reflectivity too. If θ is the angle of incidence, λ the wavelength, z the RMS roughness and R_0 the reflectivity of an ideal surface with the same coating, then the practical reflectivity is[6]

$$R = R_0 e^{-(4\pi z \cos\theta/\lambda)^2}. \qquad (1)$$

One can tolerate RMS roughness of order 20 Å at losses of $\sim$ 20% under typical conditions. Such surface finishes are easily attainable by reputable optical manufacturers in many countries.

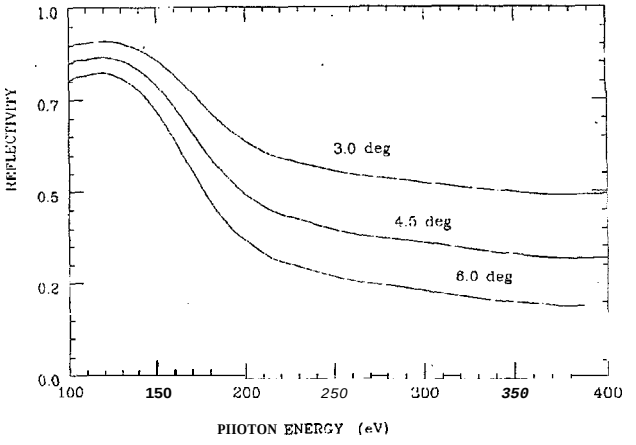

Figure 2: Reflectivity of a gold coated mirror, calculated with the computer code SHADOW.

11.2. Surface figure

A point source is imaged into a point (no aberrations) by an ellipsoid of revolution with foci at the source and image positions, and this would seem to be the ideal shape, in principle. By specifying distances r_1, r_2 to the foci and the grazing angle of incidence ϕ (see figure 3), the ellipsoid semi-axes are found to be

$$2a = r_1 + r_2, \qquad (2a)$$

and

$$2b = 2sen\phi(r_1 r_2)^{1/2}, \qquad (2b)$$

which fixes completely the mirror figure.

However, a synchrotron source is far from a point source. In fact, if the optics collects radiation coming from a horizontal fan with total aperture angle ϕ and if the electron beam orbit has a radius of curvature R, the depth d of the source is d $\approx R\phi$, which amounts to several cm in typical cases. Even if ϕ is kept small the

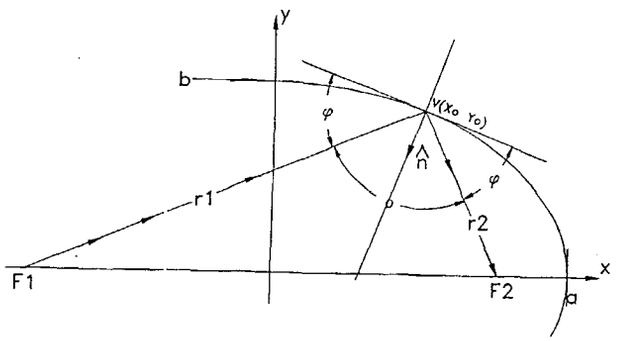

Figure 3: Geometry for an ellipsoidal mirror.

finite emittanre of the stored electron beam dictates a finite size for the focused photon beam, usually larger than current standards for consumer type optical goods (often capable of diffraction limited performance in the visible range)

From a practical point of view an ellipsoid is expensive to grind and difficult to check, because the two principal radii of curvature have values that change from point to point over the whole surface. One shows that if the ellipsoidal semi-axes are a, b and if r_1, r_2 are the foci, then the two principal radii of curvature are

$$R = \frac{1}{ab}(r_1 r_2)^{3/2}, \qquad (3a)$$

and

$$\rho = \frac{b}{a}(r_1 r_2)^{1/2}. \qquad (3b)$$

One looks therefore for a compromise solution. If the mirror collects light only over a small solid angle (as is usually the case with synchrotron light beams) we neglect the variation of R and p over the surface, and compute the curvatures for just the ray that passes through the niirror pole.

The corresponding figure is a toroid, which is much simpler to manufacture and to check.

The semi-axis lengths can be eliminated from the formulae for ρ and R, yielding the results familiar from aberration theory[7]

$$R = \frac{2}{\cos\theta}\left(\frac{1}{r_1} + \frac{1}{r_2}\right)^{-1}, \qquad (4a)$$

and

$$\rho = 2\cos\theta\left(\frac{1}{r_1} + \frac{1}{r_2}\right)^{-1}, \qquad (4b)$$

where θ is the angle of incidence for the ray passing through the mirror pole. Figure 4 shows the light intensity distribution at the focal plane of an ellipsoidal mirror illuminated by the LNLS synchrotron source, as computed by SHADOW[5]. This spot is not different

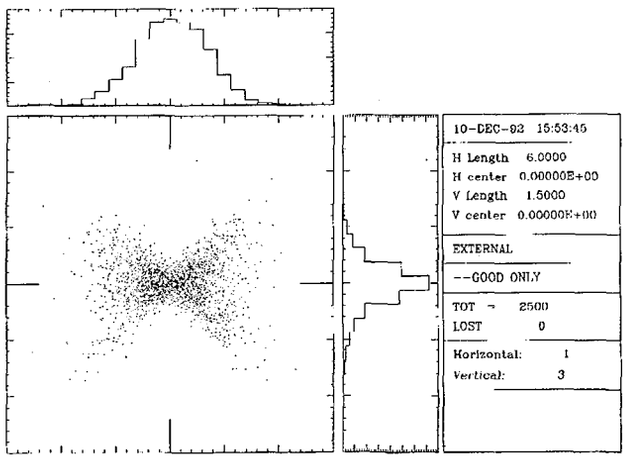

Figure 4: Focal spot produced by an ideal elliptical mirror collecting 20 mrad hor of bending magnet radiation from the LNLS synchrotron source. This is to be compared with the performance given by a toroidal mirror, figure 11. The focal spot ray distribution box is 6.0 mm long by 1.5 mm high.

from that shown in figure 11, produced by a toroidal mirror, under identical conditions. It is obvious that there is nothing to be gained by going over to the ellipsoidal geometry in this case.

Figure 5 shows a comparison between theoretical and actual performance of the toroidal mirror which serves as condenser (Mirror 1) in the beamline, under illumination from a point source. The histogram shows the intensity as a function of vertical coordinate. The data points show the intensity detected behind the focal plane, when the mirror is illuminated from a point source (focused HeNe laser beam) and a micrometer driven knife edge is run across the beam waist at the image plane. The data points are shown superimposed on a theoretical curve obtained by integrating along the vertical coordinate, the intensity given in the histogram. Mirror 2 was also tested in this same way. The practical performance of both mirrors is seen to approach the theoretical limit closely.

Toroidal gratings were initially proposed by Haber[8]. Holographically recorded toroidal gratings have been the subject of extensive research because by playing with the recording parameters it is possible to minirnize aberrations over a given spectral range[9]. LNLS bought a set of holographically recorded toroidal gratings with square grooves for this beamline. This groove shape suppresses second order and greatly attenuates third order diffraction, at the cost of a small loss in first order efficiency.

For purposes of preliminary testing, it is worthwhile to observe that any grating will in zero order perform like a mirror, for any wavelength. The grating substrate

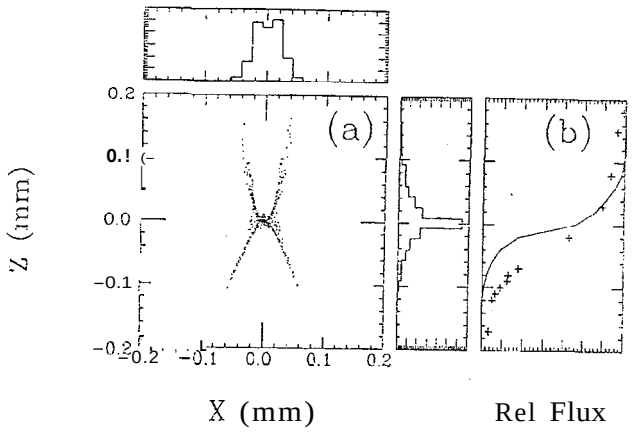

Figure 5: a) Theoretical performance of the first toroidal mirror installed on the beamline. b) Comparison between the theoretical (line) and experimental (+) performances of the first mirror. See details of the measurement in the text.

figure and the geometry of our monochromotor were tested with a focussed laser beam in the same fashion as the condensing mirrors, prior to shipping the beamline to CAMD in June 1992. Since the goal is to optimize the dispersion of soft x-rays one realizes that eq.(4a,b) are not exactly satisfied. However, given the geometry and the toroidal radii, the point spread function can be evaluated by ray-tracing and compared to the actual spot measured. Table I shows this comparison for one of the gratings in the set. The good agreement shows that the monochromator alignment procedure was successful.

11.3. Depth of focus and alignment tolerances

By "surveying" it is meant here the placement of the optical elements (mirrors, slits, gratings) at their correct coordinates in the beamline. By "alignment" it is meant here the adjustment of each optical component orientation, which might include fine ajustments in the position.

The surveying tolerances depend on the depth of focus. The photon beams in a beamline have relatively small divergences; also, they have relatively large waists, because grazing incidence optics suffers from rather large aberrations (compared to diffraction limited refractive optics for visible light). A simple estimate of the depth of focus D is given by

$$D = \omega(F/W), \tag{5}$$

where w is the minimum spot size, estimated by ray-tracing[5] or direct measurement, F is the focal distance and W some effective width of the optical eleinent. The significance of D is that the spot size will change negligibly if the image plane is moved forward or backwards by a distance D.

For the condensing mirror #1 in the TGM beamline, $w \sim 0.2$ mm, $F = 2650$ mm and W = 60 mm, yielding a depth of focus D ≅ 9 mm, which would seen to be an extremely confortable surveying tolerance.

This is a misleading conclusion. The focal distance and the quality of focal spots for grazing incidence optics depend sharply on the angle of incidence.

Starting from the "focus equation", eq.(4a), one finds for the change dr_2 in exit focal distance, when the grazing angle of incidence a changes by da, the relation

$$\frac{dr_2}{r_2} = \left(1 + \frac{r_2}{r_1}\right) cotan\ a\ da \tag{6}$$

Now, the angle of grazing incidence a is related to the distance ℓ and the offset in height h between successive optical components, by

$$\frac{da}{a} = \frac{dh}{h} + \frac{d\ell}{\ell}, \tag{7}$$

Let dx be the required accuracy in distance measurements. We set dh = dx = $d\ell$ and since for the TGM beamline $\ell \gg$ h, we write

$$\frac{da}{a} \approx \frac{dx}{h} \tag{8}$$

Now, solving for dx in terms of the "depth of focus" dr_2, one finds

$$dx = h\left(\frac{dr_2}{r_2}\right)\left(\frac{tan\ a}{a}\right)\left(\frac{r_1}{r_1 + r_2}\right). \tag{9}$$

For the monochromator components, one has r_1 = 1000 mm, r_2 ≅ 1400 mm, dr_2 ≅ 6 mm, h ~ 100 mm a = 4.5 deg. Eq.(9) then yields dx = 0.2 mm, showing that one needs high precision positioning in spite of large depths of focus. It was possible to position the gratings and slit assemblies to within ±0.3 mm of ideal distances, with the help of two theodolites and a surveying network laid out on the floor of the experimental hall.

The orientation of the toroidal mirrors and gratings is critica1 too. Ray-tracing shows that a tilt of 0.1 deg (1.7 mrad) about the grating normal broadens the focal spot and reduces the spectral resolving power by a factor of two. The effect of rotations about other axes is much less critical. It was possible to align the grating and the grating rotation axis to within ±0.7 mrad of ideal orientation.

Table I. Comparison between measured and expected spot size when the monochromator grating is set to zero-order reflection under illumination from a point source. θ is the angle of incidence, I_A is the distance to the source, I_B is the distance to the image plane.

Geometry	Theor. Width	Measured Width	Theor. Height	Measured Height
1) *Standard* $\theta = 81.0$ $I_A = 1001.6$ $I_B = 1414.3$	0.7	0.6 ± 0.2	2.3	2.5 ± 0.2
2) *Larger deviation* $\theta = 81.5463'$ $I_A = 1001.6$ $I_B = 1414.3$	4.0	3.5 ± 0.5	0.2 (waist)	0.3 ± 0.2 (waist)
3) *Larger exit distance* $\theta = 81.0°$ $I_A = 1001.6$ $I_B = 1654.8$	6.0	5.0 ± 0.5	0.25 (waist)	0.5 ± 0.2 (waist)

11.4. Optical characterization

Initial operation of the beamline was rendered very easy by the care bestowed on the surveying and alignment. In fact, it was possible to see some synchrotron light coming out of the sample chamber rear viewport (see figure 1) almost immediatly after opening all valves and shutters, on the very first trial. Later on, the light beam had to be centered a little (moved sideways by $\sim$ 2 mrn) because it was hitting a side guard in the exit slit assembly. These guards were inadvertently left very close (slit lenght $\sim$ 4 mm) and will be opened up. It is not clear at the time of this writing whether the photon beam was hitting the guard due to beamline misalignment, or because the stored electron beam might be following a displaced orbit.

Whenever it was possible to see the photon beam, its shape was very close to that expected from ray-tracings of toroidal mirrors, but careful measurements of focal spot size have not yet been done at this beamline.

A few intensity measurements have already been performed, with a stored electron beam of 4 mA, 1.2 GeV. In order to do that, a windowless Hamamatsu GaAsP - Au Schottky diode G 1127-02 was mounted to the sample chamber; its position could not be optimized, but from a nearby viewport it was visually ascertained that it intercepted most of the photon beam when the grating angle was set to zero-order reflection. The diode was connected to a Keithley digital picoammeter, on the short circuit mode.

The intensity measurements were made with both entrance and exit slits set to a width of 0.25 mm.

When the grating angle was set to zero-order reflection, a current of $\sim$ 30 μA was registered. Figure 6 shows wavelength scans made over the full range of each grating, which we now proceed to discuss.

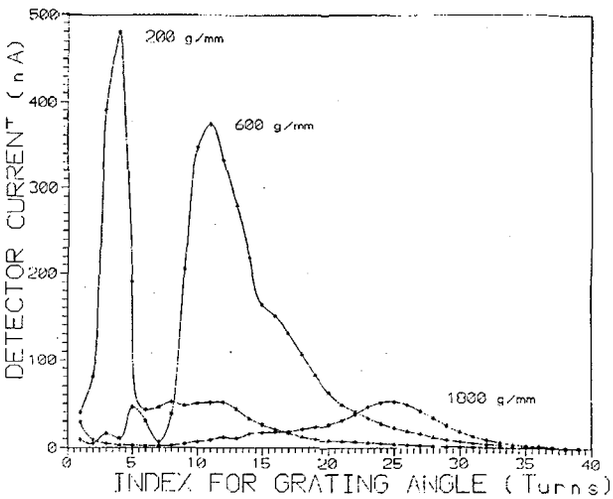

Figure 6: Spectral distributions measured during initial operation, with 0.25 mm slit widths, and with a stored beam of 4 mA, 1.2 GeV.

For the 1800 g/mm grating, one sees a smooth distribution peaked at $\lambda \sim 80$ Å. Harmonic contamination is in this case expected to be very small, because the two gold coated mirrors at 4.5' grazing incidence angle act as a low pass filter with cut off at about 40 Å. The laminar gratings are expected to suppress 2nd harmonic completely; they allow a small amount of 3rd harrnonic, but for the 1800 g/mm grating this is beyond the mirror cut off.

The peak current, at $\lambda \sim 80$ Å, was 60 nA. The photodiode responsivity, 0.17 A/W, was given by Krumrey and Tegeler[10] . One has therefore a photon flux of 1.5 x 10^{10} photons/sec.

The expected flux at this wavelength would be, for the TGM beamline 36 x 10^{10} photons/sec on a 0.1% band pass[2].

We were therefore collecting only 1/24 of the ex-

pected intensity at the sample chamber, which might most probably be due to poor focussing of the synchrotron light beam at the entrance slits. Flux, however, was a matter of concern only insofar as we were afraid of damaging the photodiode.

The spectral distributions from the other two gratings are not so nice, and there is strong evidence of harmonic contamination at the short wavelength end of the range. In addition, the responsivity of the GaAsP/Au Schottky photodiode falls sharply for photon energies below 100 eV, which makes it difficult to lend quantitative meaning to these curves. Yet, fluxes comparable to that measured at $\lambda \sim 80$ are apparently available.

Measurements to characterize the spectral resolution are under way at the time of this writing.

III. Thermal considerations

111.1. Introduction

The first mirror of the LNLS TGM beamline will collect 22 mrad hor of bending magnet radiation. When installed at CAMD[3] (1.2 GeV, 0.4 A; 4 W/mrad hor) the power incident on it will be 88 W. The power reflected will be close to 10 W. The first mirror and the slits will have to be cooled. This describes the thermal analysis of tlie mirror and slit. Also, it describes tlie modifications proposed for the mirror chamber and for the slit assembly. The conclusions are: (1) it is possible to avoid destructive heating, but (2) the focal spot at the entrance slits will be broader than in the ideal case, due to thermal distortion of the toroidal rnirror; (3) no thermal problems are expected at the grating.

111.2. Heat load on the toroidal mirror

The first mirror is on a copper-kanigan substrate 40 mm thick, with a 60 × 200 mm^2 polished face. According to the original design, which considered only a very light heat load, this block was to be clamped to a flat stainless steel table 200 mm long and 10 mm thick, supported at both ends inside a vacuum chamber. The thermal resistance of this arrangement is very high. In case of rnirror lieating, tliis layout would result in large bending moments being applied to the internal supports and to the charnber itself. The mirror temperature would be very high too. For instance, assuming the main cooling mechanism is just radiative loss, the mirror surface temperature T would be given[11] by

$$T = \left((T_{\mathrm{enc}})^4 + P/(\eta A \sigma)\right)^{1/4}, \qquad (10)$$

where $a = 5.5 \times 10^{12}$ W/cm^2°C^4 is the Stefan-Boltzmann constant, η is the emissivity, A is the surface area, T_{enc} is the temperature of the enclosure, and P is the power absorbed. Taking **P** = 88 W, $\eta = 1$, $T_{\mathrm{enc}} = 300$ K, A = 448cm^2, we get from eq.10, T = 454 K = 181 C. As a consequence, the mirror vacuum chamber was redesigned to allow for active cooling. In the new design, the mirror table is made out of copper. The center of the copper table is bolted to a water-cooled heat-sink with a cold area of 25 x 100 mm^2. Neglecting interface resistances, the thermal resistance between the inirror and the heat-sink was estimated to be less than 0.01 K/W. It would therefore contribute with less than 1 K temperature difference at a heat flux of 88W. Figure 7 shows a side view of tlie redesigned chamber. Its cylindrical wall, a section of stainless tubing, was cut in two and a copper disk 25 mm thick inserted. There are no water tubes going in or out of the vacuum enclosure.

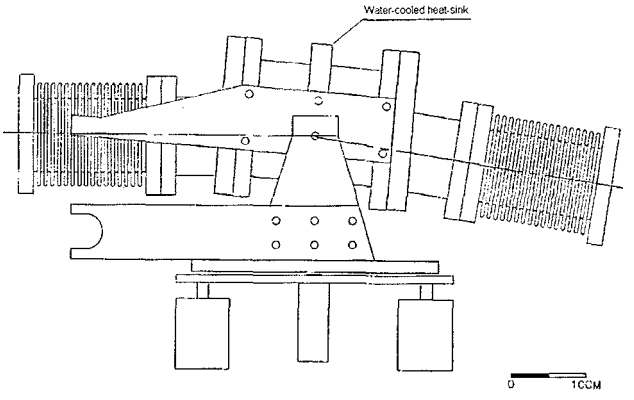

Figure 7: Mirror chamber after being redesigned for water cooling.

Next, one must address the question of what is the temperature distribution in the mirror. A finite-element calculation coupled to ray-tracing[12] was performed in order to find the temperature and strain fields. The bottom was assumed to be ideally heat-sunk to zero temperature. The heat input on the top was obtained from ray-tracing. The light source had 2500 rays and matched the spatial, angular and spectral photon distribution of the LNLS UVX ring closely. The total incident power was 88 W, the total absorbed power was 78.6 W, the total reflected power was 9.4 W and the maximum density of absorbed power was 77 mW/mrn^2. For the finite-element calculations, the toroidal concavity of the top surface was disregarded, as well as the clamping slots on the sides of the mirror block. It was also assumed that the "plane of incidence" is a plane of symmetry. The finite-element meshing extends therefore over only half of the mirror block. Figure 8 shows the mesh on the undistorted (half-) mirror block. Figure 9 shows temperature contours under full heat load. Figure 10 shows the thermally distorted (half-) mirror

block. The strain data for the top surface of the mirror (i.e, its optical surface) were then transferred back to the ray-tracing environment, and the thermally distorted mirror was ray-traced with the same source as before. Figure 11 shows the focal spot produced by an ideal toroidal mirror collecting 20 mrad hor of bending magnet radiation from the LNLS UVX ring. Figure 12 shows the effect of the thermal distortion displayed on figure 10. The spot width almost doubles, from FWHM = 0.19 min (ideal case) to FWHM = 0.36 mm (thermally distorted case).

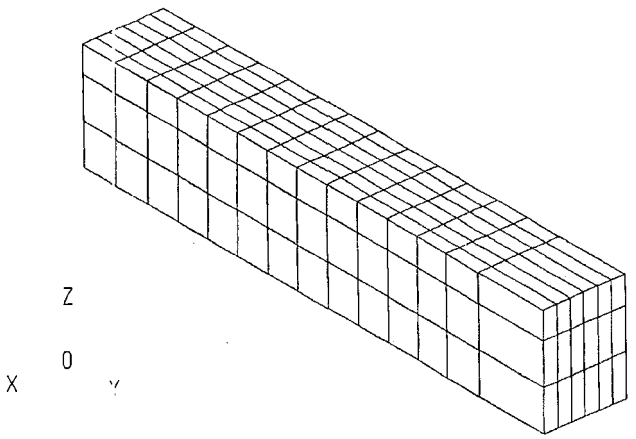

Figure 8: Mesh on the undistorted half mirror block. The object shown is *30* x *200 x 40mm*^{3} (XYZ).

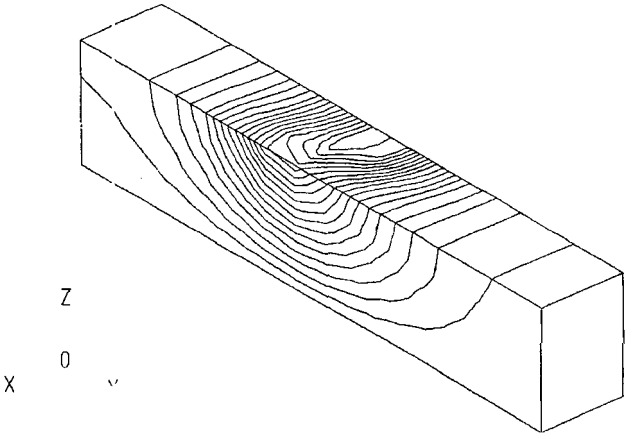

Figure 9: Temperature contours for half mirror block, under full thermal load, if mounted to the water cooled mirror chamber shown in Fig 7. The maximum temperature increase, at the center, is *2.2* deg C. The object shown is $30 \times 200 \times 40mm^3$ (XYZ).

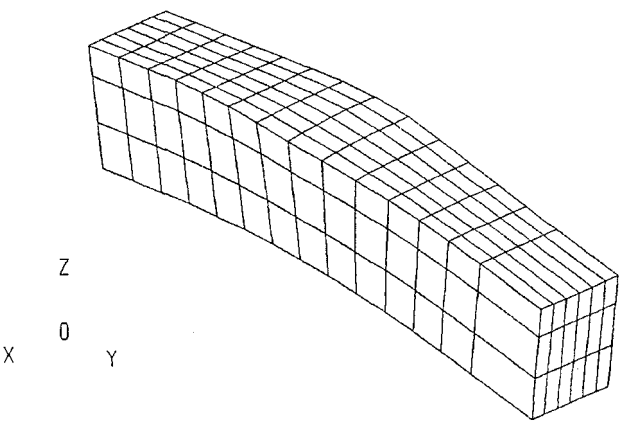

Figure *10:* Thermal distorsion of half the mirror block, due to the non-uniform temperature field shown in Fig 9. The object is *30* x *200 x 40mm*^{3} *(XYZ)*. In this figure the strains have been magnified by a factor of *5000*.

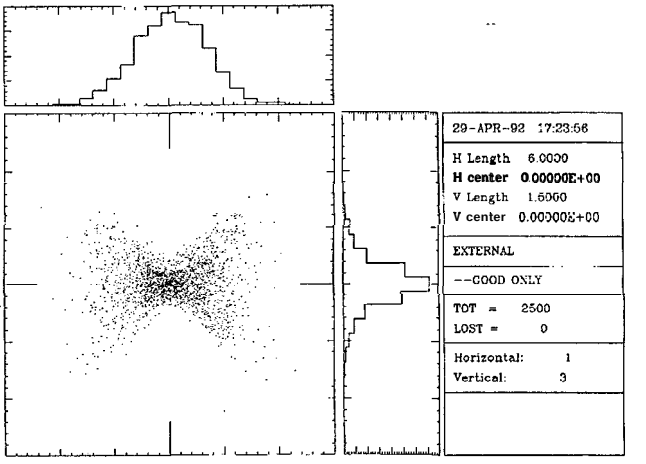

Figure 11: Focal spot produced by an ideal toroidal mirror collecting *20* mrad hor of bending magnet radiation from the LNLS synchrotron source. This is to be compared with the perforrnance given by an elliptical mirror, fig. 4. The focal spot ray distribution box is 6.0 mrn long by *1.5* mm high.

This strong disturbance in the focal spot is, in a way, unexpected. However, it is in good agreement with very simple estimates of surface figure error due to thermal bowing of the rnirror. If shear forces are neglected, if the heat flux is predominantly normal to the top/bottom surfaces and if the density of absorbed power is independent of the "sagittal" coordinate, then the total tangential bowing angle u is given by[13]

$$u = (a/k)(P/W), \qquad (11)$$

where (a/k), the ratio of thermal expansion coefficient to thermal conductivity, is a well know figure of merit for substrates of optical components, **P** is the total absorbed power and W is the width along the sagittal

direction. If, on the otlier hand, tlie density of absorbed power is a well localized function witli a bump of FWHM dL, then, undes much less restrictive conditions than given above, the total tangential bowing angle due to the "local bump" is

$$u = (a/k)jdL, \qquad (12)$$

where j is the peak value of absorbed power. Here, **P** = 78 W, j = 77 mW/mm^2, w= 60 mm, dL = 40 mm, and, for copper, (a/k) = 4.2 x 10^{-5} mm/W. Then, eq.(11) yields u= 0.054 mrad, and eq. (12), u = 0.13 mrad. The exit focal distance for the toroidal mirror is 2650 mm; tlie added spot width dz is therefore 0.14 < dz < 0.34 mm.

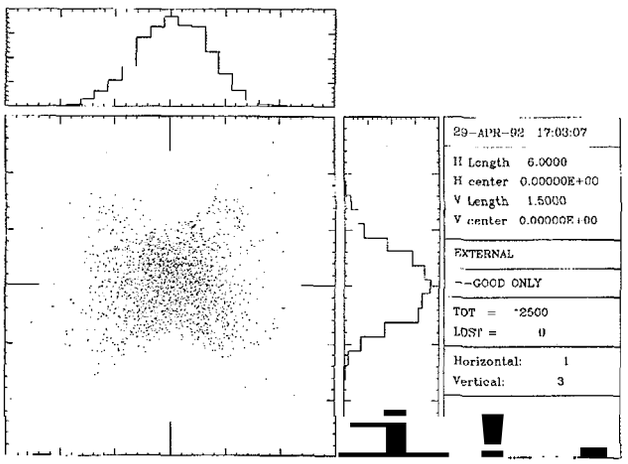

Figure 12: Focal spot produced by tlie thermally distorted optical surface of the toroidal mirror. The focal spot ray distribution box is 6.0 min long by 1.5 mm high.

Now, in order to achieve optimum spectral resolution in the TGM it is required tliat the slits be closed down to a width of circa 0.2 mm. Therefore, thermal distortion of the pre-focussing toroidal mirror translates into a loss of photon flux.

There seems to be no easy solution for this difficiilty. If, for instance, the mirror entrance focal distance is increased and the exit distance shortened in order to have a magnification less than unity, one loses flux because a smaller hor angle will be collected, and again one loses flux because the grating useful.area now will no longer match the mirror area (i.e, some photons will miss the grating). If one chooses a reflective coating with higher reflectivity for the mirror, one just transfers the problem to the slit assembly or to the grating itself.

111.3. Heat load on the entrance slits assembly

The entrance slits assembly was purchased from *Acton Research* Inc., USA. The slit blades (which *seem* to be made out of tantalum metal) are $25 \times 10 \times 2mm^3$, bolted to stainless steel carriages of intricate shape, whicli slide on steel balls. Thermal contact between tlie carriages and tlie stainless steel supporting structure (or between the latter and the mounting ConFlat flange, for tliat matter) is very poor. The meclianism is ratecl for operation at up to 150C. If tlie focussed beam misses tlie aperture and hits one of the jarvs, considerable lieating is expected. Assuming only radiative cooling, talíing p = 9.4 W, A = 20 cm^2, eq.10 leads to T = 548 K = 275 C, a temperature that might jam the meclianism and cause a considerable rise in pressure due to tliermal desorption. It is therefore considered that active cooling of tlie slit jaws is needed. A cold finger can be instnlled on the same ConFlat that liolds the mechanism and the linear feed-through used to adjust the slit widtli. Copper plates with a harness of fine copper wires would establisli a thermal path from the slit jaws to the cold finger. Assuming tlie harness of fine copper wires has an effective cross-sectional area A = $15mm^2$ and a lenght L = 40 mm, tlie thermal resistance is R = 6.7 K/W. The temperature difference across the harness, at a heat flux of 9.4 W, will be 63 C, which will keep the mechanism at a safe temperature below the 150 C upper limit.

The temperature distribution on the jaw itself was also studied with finite elements. The heat input distribution, also taken from ray-tracing, is actually given in figure 11. The mesh used covers a full blade (no symmetry plane in this case), and simplifications regarding the geometry of the block, as well as the boundary conditions, were made in this case t o ~ Figure 13 and 14 show the temperature distribution and the thermally distorted blade, when the light spot is incident on the blade top surface, 0.5 mm away from the edge, and the bottom surface is kept at a uniform temperature. The highest temperature, for a tantalum blade, would be 73 C above the bottom temperature, which would seem safe. The thermal strain would amount to about 0.002 mm which is negligible compared to a minimum slit width of 0.2 mm. Notice, however, that the strain just mentioned is unrelated to changes in slit width caused by "uniform" heating of the carriage and jaws. Given the layout of the parts, expansions of the carriage and jaw would partially cancel out. An upper bound would be obtained by considering the expansion of just the tantalum jaw. Assuming an average temperature increase of 100°C, taking L= 5 mm, a = 6.5 x 10^{-6}, one finds dL = 0.003 mm, also negligible under typical conditions of usage for the TGM *beamline*.

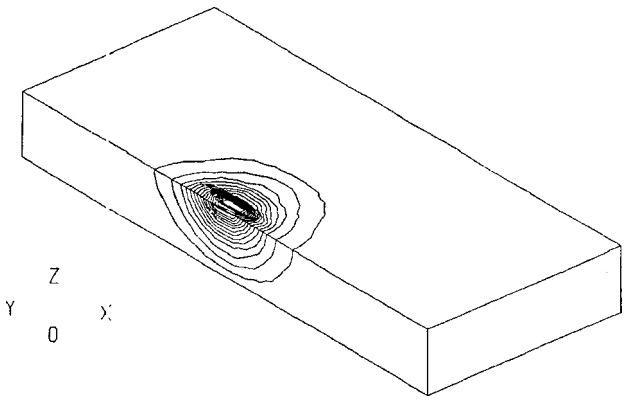

Figure **13:** Temperature distribution on a slit jaw under heat load. The highest temperature increase (center contour) is *72.5* deg C. The object shown is **10** x *25* $\times$ $2mm^3$ (XYZ).

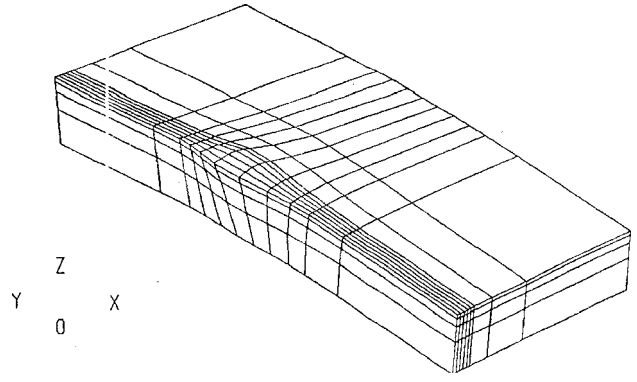

Figure **14:** Strain field on a slit jaw, due to the non-uniform temperature distribution shown in Fig **13.** The object shown is 10 x *25* **x** $2mm^3$ (XYZ). In this figure the strains have been magnified by a factor *2000.*

111.4. Heat load on the gratings

The absorption on the gratings should be small, since most of the high energy photons were filtered out at the toroidal mirror. So, a rough estimate should suffice. Assume 5 W are absorbed, out of a maximum incident power of 10 W. The only cooling mechanism available for the gratings is radiative. The radiator surface area includes the exposed area of the grating block plus mounting hardware. This surface area is estimated to be no less than 170 cm^2. Then, eq.(10) yields T = 339 K = 66 C, which seems safe because the gratings can supposedly be baked out at 150 C.

It was assumed so far that the entrance slits are wide open, in which case, of course, it does not make any sense to worry about loss of spectral resolution due to thermal distortion of the grating. However, let us do worry about spectral resolution. Then the entrance slits must be closed down to, say, 0.2 mm width, and looking at figure 2, it is obvious that about half of the incoming power will be blocked by the slits. Our estimate of power absorbed on the grating must now be halved to something like 2.5 W. The width of the illuminated region will be 23 mm, while its length will depend on grating angle setting. For fused silica, $(a/k) = 3.9 \times 10^{-4}$ mm/W. Now, using eq.(11), we get for the surface figure error u = 0.043 mrad. The exit focal distance is 1414 mm, yielding for the added spot width at the exit slits only 0.06 mm. This is negligible compared to typical aberration limited spot widths of more than 0.15 mm.

In conclusion, the LNLS TGM beamline will be operating at its limits when installed at CAMD. There should be no disastrous thermal effects, but it will not be able to exploit to full advantage the plioton flux that is expected at maximum injected current.

IV. Soft X-ray emission applications

IV.1. The LNLS VUV spectrograph

The VUV Spectrograph built at LNLS is a scaled down version of the instruments described by Nordgren and Nyholm[14] and by Calcott, Tsang, Zhang, Ederer and Arakawa[15].

It covers the spectral range 30 eV - 150 eV with a single holographic toroidal grating, affording a maximum resolving power of about 500. The grating accepts a solid angle of 644 $(\text{mrad})^2$ [16].

Figure 15 shows an outline of this instrument.

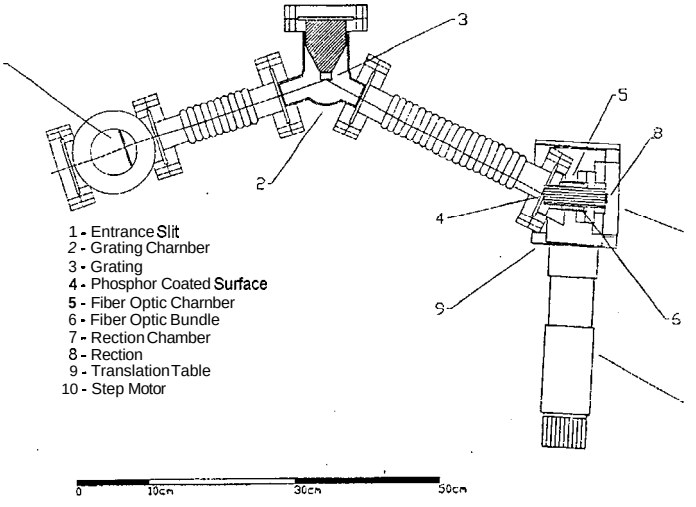

Figure *15:* Outline of the VUV Spectrograph built at LNLS.

The entrance slit assembly was designed to allow close approach ($\sim$ 2 mm) to the sample. The slit height is 2 mm, while the width can be pre-selected (0.1, 0.2, 0.5 mm) before evacuating the system.

The focal plane detector comprises a 25 mm diameter fiber optic bundle mounted to a ConFlat flange plus a diode array. The UHV side of the optical bundle, which is at the grating focal plane, has a thin phosphor coating which fluoresces under VUV excitation. The visible fluorescence is coupled out to the atmosphere side of the fiber optic bundle, which is in direct contact with the fiber optic face plate of a thermoelectrically cooled EGG Reticon RL512SF diode array. The drive electronics for the diode array has been described elsewhere[17] . It was slightly rnodified to allow usage of LNLS standard digital modules, and more straightforward serial connection to microcomputers. The estimated sensitivity threshold of the photometric system is 3×10^5 UV photons at the entrance slit within a relative bandwidth of 0.2%[16] .

The detection system slides on a step motor driven translation stage (40 mm course) for selection of the spectral band. It is connected to the grating chamber by a bellows of welded diaphragms.

The complete spectrograph is mounted on a large XYZ table; a second bellows, approximately coaxial with the entrance slit assembly, connects to the sample chamber and allows for precise positioning of the entrance slit with respect to the sample.

Preliminary optical testing was conducted by installing a comercial UHV slit assembly in place of our own assembly, and looking at the zero-order reflection from the grating, under visible light excitation. A focus with about 0.1 mm width (FWHM) was measured, in excellent agreement with estimates made using ray-tracing.

Further testing was done with a windowless He lamp. Figure 16 shows the zero order lineshape recorded, with a FWHM 0.12 mm, very close to the expected instrumental width.

This instrument will be mounted to the sample chamber of the LNLS TGM beamline at CAMD, USA, in Dec 1992.

IV.2. Introduction to soft X-ray emission

The two basic methods of studying the electronic structure of atomic core states are x-ray fluorescence and photo-electron spectroscopy. The physical processes involved in these techniques are, roughly speaking, one inverse to the other. However, in X-ray fluorescence the initial and final states are discrete while in photo-electron spectroscopy the final state is in the continuum. The matrix elements for a fluorescent transition are more sharply restricted by the dipole selection rules than the corresponding photoeffect transition, because in one case, one deals with well localized orbitals for both initial and final states while in the other case one of the states is unbounded. Such differences suggest that these techniques should yield complementary data.

Both techniques have been applied to study beryllium and boron, which present great interest because their electronic shells, (1s)2(2s)2 and (1s)2(2s)2(2p) respectively, are sufficiently simple to allow for rather complete theoretical studies, yet subtle enough to allow for very rich chemical behavior and non-trivial physical phenomena.

Beryllium metal and Be0 have widespread application in the nuclear power industry, in instrumentation for X-rays and in electronics. Boron is a component of advanced magnetic alloys and a dopant for 111-V and other semicondutors. It is used in the form of fibers to reinforce high strength structural materials. The chemistry of boron is unique. This is the only non-metal with 3 valence electrons; the resulting covalent bonding leads to compounds such as BN and B_4C, hard and refractory materials of technical importance. Calculation of the electronic structure of these atoms has been a subject of interest for some time[18] . More recent calculations have focussed on the solid state properties of icosahedral B12 [19] and on the properties of ionized radicals[20,21].

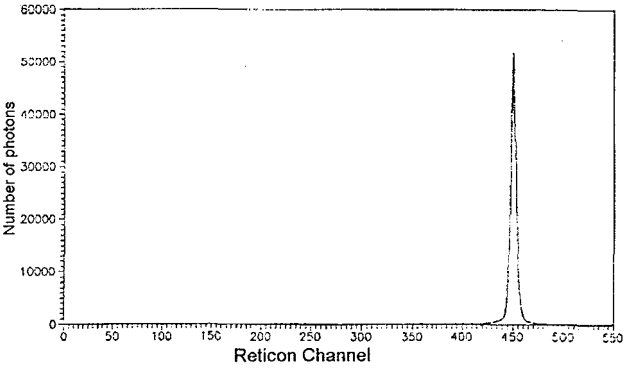

Figure 16: Zero order lineshape recorded with the LNLS VUV Spectrograph and a windowless He lamp.

IV.3. X-Ray Fluorescence of Boron

Luck and Urch[22] have studied the K alpha emission of boron compounds, finding satellites both below and above the main peak. In addition, there are shifts in the position of the main peak and very noticeable changes in line shape. The authors discuss the origin of the satellites, but there remain discrepancies with previous results of other workers, regarding the relative intensities.

The data of Luck and Urch which have just been mentioned might be limited by signal to noise ratio and by instrumental bandwidth. The measured linewidths are often larger than 5 eV, which is larger than the width measured in photoelectron spectroscopy[23]. It is proposed to measure the X-ray fluorescence of boron and several compounds using SR excitation and a spectrograph with bandpass narrower than the linewidths so far reported. It is desired to pay particular attention to the energy shifts, which reveal the degree of covalency in the bonds. It is expected that the line position should shift by about 1 eV when going from purely metallic to ionic bonding[24] . Materials to be studied would include crystalline boron, hBN, cBN, B_4C and B_2O_3.

IV.4. X-Ray Fluorescence of Berlyllium

Since the electronic shell of beryllium is (1s)2(2s)2, fluorescent transitions to a 1s hole are forbidden by dipole selection rules. However, the 2s electrons might acquire some 2p character in compounds, due to hybridizatior of the wave function. The excited states of this atom might also have 2p character. In fact, Caldwell and coworkers[25] report the observation of an excited (1s)(2s)2(2p) state that, nevertheless, decays into Be+ (1s)2(2s) (2p) with high probability in their atomic beam experiments. Hessabi and Urch[26] report the observation of Be K alpha emission in BeF (and in other alkali-metal fluorides), but their emphasys was really on the prcperties of the F levels. An interesting question is whether the process observed by Caldwell et al. is quenched in crystalline beryllium, in which case the decay from the excited state might include soft X-ray emission.

If the sample is photo-excited near the 1s - 2p transition one would expect a sensitive dependence of the soft X-ray yield as a function of the exciting photon energy.

Questions of line shift and line profile as a function of the chemical species attached to the Be atom can also be addressed. Materials to be studied would include Be crystals, BeF and BeO.

IV.5. Estimate of fluorescence signal strength

The factors affecting signal strength are: (1) photon flux at the sample; (2) sample fluorescent yield; (3) collection efficiency, which is a function of the solid angle of collection, grating efficiency, and detector head photometric efficiency. In the following part we will try to discuss each factor but only a rough estimate will be attempted.

For boron K alpha studies (ernission at 188 eV) one might excite at 200 eV, while for berlyllium K alpha (112 eV) one might use 120 eV. The photon flux at the sample, for the LNLS TGM beamline, can be estimated at 9×10^{12} (120 eV) and 5×10^{12} (200 eV) photons/sec on a 0.1% bandwidth (1.15 GeV, 100 mA)[2]. If this beamline is installed at CAMD, which is to be operated at 400 mA, one would expect 2×10^{13} (200 eV) and higher at 120 eV.

The fluorescent emission yield is limited by competing non-radiative decay processes to typically 0.1%[27] . We expect, therefore, a total fluorescent flux of 2×10^{10} if one excites at 200 eV and higher if excited at 120 eV.

The spectrograph entrance slits are $1.0 \times 0.1 mm^2$. If the sample is 5.0 mm away and if one assumes almost isotropic emission over 2π sterrad from a point source, then the fraction of the fluorescent emission entering the spectrograph is 6.4×10^{-4}, which matches the angular acceptance of the spectrograph exactly. The photon flux at the grating is then 1.3×10^7 (UV photons)/sec and higher if excited at 120 eV.

The grating efficiency and the photometric sensitivity of the detector head have also been discussed[16] . Exposures of 200 sec/frame can be accomodated by cooling the detector head. So, we expect a fluorescent count of 2.6×10^9 (UV photons) to be available upstream of the grating. Due to the angles and wavelengths involved, the reflectivity efficiency of the gold coated grating is expected to be a factor of 20 smaller at 188 eV than at the center of the nominal spectral range of operation (we take an overall grating efficiency of 1%). On the other hand, vignetting losses due to stigmatism are negligible for the flat field grating. We expect a fluorescent count of 2.6×10^7 (UV photons) to be available at the phosphor coating of the detector head, much higher if working at lower photon energy.

Finally, it is necessary to estimate how many diodes will be illuminated by the available photons. For the boron K alpha emission (188 eV, 66 A), widths of 2.1 A were observed[22] . Using a linear dispersion D = 5.64 A/mm[16] and a diode spacing of 0.025 mm, one finds that 15 diodes would be illuminated. So, one expects about 1.7×10^6 (UV photons)/diode at the phosphor layer.

The phosphor coating downconversion efficiency at 188 eV (66 A) is about 1.5 (visible photons) / (UV photon). Then, assuming ideal coupling of visible light to the Si substrate, one expects 1.5 (electronic charges) / (UV photon). The detector read-out noise is 1500

(electronic charges) / diode, which leads to a threshold for detection of 1000 (UV photons) / diode.

The signal of 1.7 x 10^6 (UV photons) / diode is 3 orders of magnitude larger than tlie threshold for detection. In addition, tlie signal to noise ratio can be furtlier improved by signal averaging (adding multiple frames).

In tlie case of beryllium K α (112 eV), tlie exciting flux is larger, the grating efficiency is much larger, tlie phosphor downconversion efficiency is somewhat sinaller, and tlie spectral width is perliaps twice as large as in the case of boron. The net result is that the signal should still be orders of magnitude larger than the threshold for detection, if the fluorescence yield is the same as for boron.

V. Conclusion

In conclusion, a beamline for the spectral range 12 eV - 310 eV has been built by LNLS and installed at CAMD/LSU, USA.

Surveying criteria and tolerances were worked out at LNLS and resulted in easy, successful operation on the first exposure to synchrotron light.

Heat loads on tlie first mirror, slits and gratings were studied with ray-tracing and finite-eleinent-analysis. No degradation in spectral resolution is expected at 0.4 A,1.2 GeV stored beam, but flux will not be optimum due to thermal distortion of the first mirror.

A VUV Spectrograph has also been built and will be mounted to tlie beamline in the near future. Soft X-ray fluorescence measurements on beryllium and boron compounds have been planned for the next months.

Acknowledgements

The authors are grateful to CAMD/LSU for the opportunity of installing and operating this beamline there, to LNLS for the continued support which made this project possible, and to Secretaria da Ciência, Tecnologia e Desenvolvimento Econômico do Estado de São Paulo for financia1 help.

It is acknowledged, with pleasure, that precision adjustable supports, UHV chambers and fittings were expertly machined at the LNLS shop; welding was done at the LNLS Vacuum Lab which also advised us on UHV cleaning and bake-out procedures; digital control equipment (LOCO modules) was supplied by the LNLS control group.

We thank M. Marino for painstaking word-processing of the manuscript.

The first author wishes that no agency derives military benefit from this paper.

References

1. Accelerator Physics and Instrumentation Groups of LNLS, Rev. Sci. Instrum., 63, 1573 (1992).
2. P. T. Fonseca, J. G. Pacheco, E. d'Vila Samogin and A. R. R. de Castro, Rev. Sci. Instrum., 63, 1256 (1992).
3. B. C. Craft, M. Feldman, E. Morikawa, E. D. Polialtoff, V. Saile, J. D. Scott, Rev. Sci. Instrum., 63, 1561 (1992).
4. J. G. Pacheco, P. T. Fonseca, A. R. B. de Castro, Rev. Bras. Apl. de Vac. 10, 151 (1991).
5. B. Lai, K. Chapman and F. Cerrina, Nucl. Instrum. Meth., **A266**, 544 (1988).
6. K. Nakajima and S. Aoki, in Proc. Intl. Symposium of X-ray microscopy, Opt. Sciences Series (Springer-Verlag, Heidelberg, 1987) Vol. 56.
7. M. Born and E. Wolf, *Principles* of *Optics*, (Pergamon Press, London, 1970) 4^{th} Edition, ch. V.
8. H. Haber, J. Opt. Soc. Am., 40, 153 (1950).
9. W. R. McKinney and C. Palmer, Appl. Opt., 26, 3108 (1987).
10. M. Krumrey and E. Tegeler, Rev. Sci. Instr., 63, 797 (1992).
11. R. Siegel and J. R. Howell, *Thermal* Radiation Heat Transfer, (Hemisphere Pub. Corp., New18. York, 1981) 2^{nd} ed.
12. "Interfacing SHADOW to the finite-element analysis environment MODULED", A. R. B. de Castro, LNLS Tecnical memo CT-01/Jan, 1992.
13. A. K. Freund, F. de Bergerin, G. Marot, C. Riekel, J. Susini, L. Zhang and E. Ziegler, Opt. Eng., 29, 928 (1990).
14. J. Nordgren and R. Nyholm, Nucl. Instr. and Meth., **A246**, 242 (1986).
15. T. A. Calcott, K. L. Tsang, C. H. Zhang, D. L. Ederer, E. T. Arakawa, Rev. Sci. Instrum., 57, 2680 (1986).
16. A. R. B. de Castro, Physica Scripta, A41, 499 (1990).
17. A. R. B. de Castro, P. T. Fonseca and J. E. Verdugo in "Festschrift in honor of Rogério Cerqueira Leite", ed. by M. Balkanski, C. E. T. Gonçalves da Silva and J. M. Worlock (World Scientific Publ., Singapore, 1991).
18. H. F. Schaefer III, The electronic *structure* of atoms and molecules - *A Survey* of rigorous *Quantum* Mechanical Results, (Addison Wesley, London, 1972).
19. S. Lee, D. M. Bylander and L. Keinman, Phys. Rev., B42, 1316 (1990).

20. P. J. Bruna and J. S. Wright, J. Phys. B: At. Mol. Phys. **23,** 2197 (1990).
21. P. L. Bruna and J. S. Wright, J. Chem. Phys., **93,** 2617 (1990).
22. S. Luck and D. S. Urch, Physica Scripta 41, 970 (1990).
23. R. Trehan, Y. Lifshitz and J. W. Rabalais, J. Vac. Sci. and Technol., **A8**, 4026 (1990).
24. R. Theisen *Quantitative electron Microprobe Analysis* (Springer-Verlag, New York, 1965).
25. C. D. Caldwell, M. G. Flemming, M. O. Krause, P. van der Meulen, C. Pan and A. F. Starace, Phys. Rev. **A41,** 542 (1990).
26. R. Hessabi and D. S. Urch, J. Chem Soc. Faraday Trans, 86, 247 (1990).
27. J. Nodgren, G. Bray, S. Crarnrn, R. Nyholm, J. E. Rubensson and N. Wassdahl, Rev. Sci. Instrum., 60, 1690 (1989).